Preparation and Performance Characterization of a new dust suppressant with a cross-linked network structure for use in open-pit coal mines

Hu Jin
Shandong University of Science and Technology
Yansong Zhang (zys6407@sdust.edu.cn)
Shandong University of Science and Technology https://orcid.org/0000-0002-1048-9140
Nan Li
Shandong University of Science and Technology
Junjie Yang
Shandong University of Science and Technology
Ya Xi
Shandong University of Science and Technology
Li Cai
Shandong University of Science and Technology
Zhichao Pan
Shandong University of Science and Technology

Research Article

Keywords: Cross-linked polymer, Control environmental pollution, Characterization dust suppressant, Graft copolymerization, Renewable polymer material

Posted Date: March 23rd, 2021

DOI: https://doi.org/10.21203/rs.3.rs-335111/v1

Abstract

In an effort to control dust pollution in open-air environments such as pit coal mines and coal transportation systems, a new dust suppressant with a cross-linked network structure was prepared. Graft copolymerization of soy protein isolate (SPI) and methacrylic acid (MAA), using potassium persulfate (KPS) as the initiator and hexametaphosphoric acid (SHMP) as the cross-linking agent, formed the network structure. The optimal MAA/SPI mass ratio for the dust suppressant was determined through a single factor experiment to be 3:4, with 0.8 and 0.2 g of SHMP and KPS, respectively. The grafting reaction required 30 min at 60 ℃. Scanning electron microscopy, energy-dispersive x-ray spectroscopy, Fourier-transform infrared spectroscopy, and differential scanning calorimetry were used to characterize the structure and application performance of the dust suppressant. The experimental results showed that the graft copolymerization reaction successfully formed the desired cross-linked network, and that when the cross-linked network material was sprayed on coal dust it formed a dense, solidified shell, which effectively resisted wind erosion and served as a dust suppressant. The average reduction of the total suspended particulate matter of an open-air coal pile reached 79.95%, demonstrating effective dust suppression.

1. Introduction

China is one of the countries where coal is the main power source. In the future, coal will still play a major energy role in China. North China is China's main coal mining area, and the coal produced is stacked in open-air coal storage yards [1–4]. Due to the cold and dry climate and strong wind in northern China, it is easy for coal dust piled in the open air to be blown by the wind, forming a source of air pollution [5–7]. Coal dust pollution has a great impact on the surrounding buildings of the coal yard, the health of residents, and their productivity and quality of life. Additionally, during the transportation of a coal pile by railway or by trucks, coal dust can be blown off the pile and spread to the surroundings. The lost coal creates air pollution and causes a serious waste of coal resources and economic losses [8–10].

To alleviate the air pollution caused by dust in coal storage yards and coal transportation processes, enterprises often spray water on the coal pile to keep its surface moist and to prevent pulverized coal from becoming airborne. However, coal is hydrophobic and the water on the coal evaporates quickly in an open-air environment. Thus, the dust suppression effect is limited. In recent years, dust suppression materials have become one of the research hotspots in the field of dust suppression [11–14]. Saha et al. [15] used calcium $CaCl_2$ and $MgCl_2$ a as dust suppressors to reduce dust pollution on roads in Wyoming. Huyao et al. [16] synthesized a liquid starch-based dust suppressant gelatin copolymer by grafting polyacrylic acid on potato starch pretreated with NaOH, and then crosslinking the graft. The dust suppression agent was characterized by Fourier transform infrared spectroscopy, thermogravimetric analysis, viscosity and contact angle measurement. Compared with spraying water, the total dust suppression rate was increased by 25% and 33%, respectively. Xie et al. [17] have developed two kinds of compound dust suppressants with excellent dust suppression performance in response to the problem of dust during transportation in open-pit mines. The mass fractions of starch, sodium dodecylbenzene

sulfonate and glycerol in No. 1 composite dust suppressant were 1.0%, 1.0% and 0.6% respectively; in No. 2 composite dust suppressant, starch, sodium polyacrylate sol, acrylic The mass fractions of triol are 0.2%, 0.2% and 0.4%, respectively. The effective dust suppression time of No. 1 dust suppressant is 4 h, and the effective dust suppression time of No. 2 dust suppressant can reach 6 h. Li et al. [18] have developed a composite dust suppressant for bulk coal. The dust suppressant has a consolidation time of 5 hours, a consolidation thickness of 23mm, and a compressive strength of 249 kPa. The use of dust suppressants can save 50% of coal dust Economic losses. With the increasing awareness of environmental protection, the use of traditional chemical dust suppressants that have deficient performance, toxicity, and the potential for pollution hazards to the environment has been gradually declining. Green, pollution-free, and environmentally friendly dust suppressants are the current research theme.

In view of this, a new dust suppressant for use in open-pit coal mines has been synthesized with graft copolymerization so that it has a cross-linked network structure. The main material selected in the experiment is soy protein isolate (SPI), which has abundant sources, low cost, and biodegradability [19, 20]. It plays an important role in the development of environmentally friendly materials. SPI is extracted from soybeans. Soybeans are one of the most important crops in the world. Soybeans are produced all over the world. Among them, North America, South America, and Asia have larger planting areas. The soybean producing countries are the United States, Brazil, Argentina, and China. In 2019, global soybeans were 342 million tons, and the output of main producing countries is shown in Fig. 1 [21]. SPI has wettability, dispersibility, and low viscosity, and its molecular interaction with proteins can lead to aggregation and gel film formation. SPI forms a three-dimensional network through hydrophobic interactions, electrostatic interactions, or hydrogen bond or disulfide bond cross-linking [22–24]. The structure and function of SPI have far-reaching practical significance. Therefore, we used SPI as our primary material, and we copolymerized it with methacrylic acid (MAA) by using potassium persulfate (KPS) as an initiator and sodium hexametaphosphate (SHMP) as a cross-linking agent. The graft copolymerization made a dust suppressant that effectively suppressed dust pollution in an open-air environment. We characterized its performance and tested its dust suppression capability in a field application[25–27].

2. Preparation And Performance Characterization Of Dust Suppressant

2.1 Materials

Soy protein isolate (SPI), methacrylic acid (MAA), potassium persulfate (KPS), potassium hexametaphosphate (SHMP), sodium hydroxide and uric acid (Urea) were all provided by Shanghai Maclean Biochemical Technology Co., Ltd. Sodium dodecyl sulfate (SDS) is provided by Shandong Yousuo Chemical Technology CO. Ltd, Shandong, China. The coal dust used in the experiment was collected near the Xinglong Zhuang coal yard of Shandong Mining Group.

2.2 Preparation of Dust Suppressant with Cross-Linked Structure

(1) Preparation of SPI dispersion: A measured amount of SPI solid powder was dispersed in a urea solution and stirred at room temperature for 1 h until the SPI was completely dissolved.

(2) Preparation of MAA solution with a degree of neutralization of 50%: NaOH (2 g) was weighed in a beaker on an electronic balance, and 10 mL of water was added to the beaker containing NaOH. The mixture was stirred evenly with a glass rod until the NaOH completely dissolved. The NaOH solution was allowed to cool to room temperature. An equal amount (10 g) of a XX% solution of MAA in water was added to the to the NaOH solution to make the final MAA solution.

(3) Synthesis of dust suppressant: Add the MAA solution with a degree of neutralization of 50% to the SPI dispersion, stir with a magnetic stirrer for 30 min, and gradually increase the temperature to 60°C. Then, add a measured amount of cross-linking agent SHMP and initiator KPS with stirring at a constant temperature of 60°C for a desired period of time. After the solution in the beaker has fully reacted, it is cooled to room temperature to complete the preparation of the dust suppressant with a cross-linked networked structure. The dust suppressant is sprayed on the surface of coal dust and the dust suppression effect is observed. The preparation process is shown in Fig. 2.

2.3 Viscosity and Compressive Strength Test

Viscosity and compressive strength are two important indicators to determine whether a dust suppressant is practical. In this experiment, the viscosity and compressive strength of the dust suppressant were used as the standards to evaluate the synthesis process conditions. The experiment used an NDJ-79 rotary viscometer and a WDW-200E universal testing machine to test viscosity and compressive strength, respectively. Using the single-variable control method, the effect of the mass ratio of the MAA and SPI monomers, the amount of initiator, the amount of cross-linking agent, the grafting reaction temperature, and the reaction time on the viscosity and compressive strength of the dust suppressant were studied.

2.4 Scanning Electron Microscope (SEM) and Energy-Dispersive X-ray Spectroscopy (EDS) Analyses

Using APREO scanning electron microscope, the surface morphology of the synthesized inhibitor and the surface morphology of the cured shell formed by the inhibitor on the surface of the medium were observed. Take a small amount of processed samples and put them into SEM. Adjust the magnification, select the appropriate field of view, and take the image of the sample particles. Meanwhile, perform an EDS test on the solidified shell formed by SPI powder and sprayed coal dust suppressant. Perform the qualitative and semi-quantitative analysis by using EDS element imaging.

2.5 Fourier-Transform Infrared Spectroscopy (FTIR)

SPI, SPI-MAA intermediate products, and SPI-MAA-SHMP synthetic dust suppressant were tested using the Nicolet iS50 infrared spectrometer (Thermo Fisher Science). The dried product is ground into a powder, and then the sample powder and KBr are uniformly mixed in a ratio of 1:100 and pressed into a thin layer, which is placed in the instrument for scanning. The scanning range is 500-4000cm^{-1}.

2.6 Differential Scanning Calorimetry (DSC)

The DSCI differential scanning calorimeter (Mettler) was used to test the liquid and solid state of the three SPI substances. Take a 10 mg sample and press it in an aluminum box. Use a blank aluminum box as a control under nitrogen protection. The heating rate is 10°C /min, the scanning starting temperature is 25°C, and the temperature is raised to 150°C to obtain the DSC curve.

2.7 Measurement of Dust Suppression Efficiency for a Coal Pile in Open Air

To test the actual dust suppression effect of the dust suppressant, two identical coal piles were stacked in the open air. The design dimensions were: 30 cm diameter on the bottom surface, 15 cm diameter on the top surface, and 10 cm height. A monitoring point for the concentration of total suspended particulate matter (TSP) in the atmosphere is set 2m downwind from the coal pile in the control group, which is monitoring point 1. No treatment is done on the surface of the coal pile. Two monitoring points of total suspended particulate matter (TSP) concentration are arranged in the test coal pile, among which monitoring point 2 and monitoring point 3 are respectively located at 2 m away from the coal pile in the upwind and downwind direction of the coal pile. The spraying amount is uniform according to 0.5 L/m^2 spray the dust suppressant solution. The monitoring time is 2020/11/2-2020/11/5, from 8 am to 18 am every day. Data is collected every two hours.

3. Experimental Results

3.1 Analysis of the Influence of Single Factors on the Adhesion and Compression Performance of Dust Suppressants

Under the condition when other factors unchanged, the influence of each single factor on both the viscosity and the compressive strength of the dust suppressant were measured, and the experimental data was fitted. The results of the data fitting are shown in Fig. 3.

Figure 3a shows the effect of the mass ratio of the MAA and SPI monomers on the viscosity and compressive strength of the synthesized dust suppressant. It can be seen that the monomer mass ratio has a great influence on the viscosity and the compressive strength. As the volume ratio increases, the viscosity and compressive strength values first increase rapidly and then their rate of increase slows. Because acrylic monomers agglomerate very easily, the use of too much MMA will affect the stability of the solution. The inflection point of the curve where the growth rate slows is at an MAA/SPI mass ratio of 3:4. The viscosity value at this mass ration is 69 mPa·s, and the compressive strength is 0.88 MPa.

Therefore, when the MAA/SPI mass ratio is 3:4, the dust suppressant has good adhesion and compression performance.

The effect of the amount of cross-linking agent on the viscosity and compressive strength of the dust suppressant is shown in Fig. 3b. As the amount of cross-linking agent increases, the viscosity first increases, and then at 0.8 g, the viscosity begins a gradual decrease. At 0.8 g the increase in the compressive strength slows. As the amount of the cross-linking agent increases beyond 0.8 g, the data point where the cross-linking occurs increases. During the cross-linking reaction, the gaps between the dust suppressant networks become smaller. As a result, it is difficult for water to enter these spaces, the degree of cross-linking decreases, and the viscosity decreases. Therefore, the selected amount of cross-linking agent is 0.8g.

Figure 3c shows the influence of the amount of initiator on the viscosity and compressive strength of the dust suppressant. As the amount of initiator increases, both the compressive strength and the viscosity first increase and then decrease. Based on the analysis, as the amount of initiator increases, the concentration of free radicals in the solution increases, and the grafting points of SPI chains increase. This increases the entanglement between molecular chains, causing the viscosity and compressive strength to increase sharply. When the amount of KPS is > 0.2 g, the molecular chain entanglement decreases. As a result, the increase in viscosity diminishes, and a downward trend appears. The compressive strength value decreases first and then increases slowly. Therefore, 0.2 g KPS is appropriate for the synthesis of the dust suppressant.

The effects of the grafting reaction temperature and time on the viscosity and compressive strength of the dust suppressant are presented in Fig. 3d, e. As the reaction time and temperature increase, the viscosity and compressive strength first increase and then become stable. When the reaction temperature is 60 ℃ and the reaction time is 30 min, the grafting reaction reaches completion. As the reaction time and temperature continuously increase beyond these levels, the viscosity and compressive strength of the dust suppressant do not increase appreciably. Therefore, the best grafting reaction condition is at 60°C for 30 min.

By testing the viscosity and compressive strength of each single factor, the best process conditions for the synthesis of dust suppressants have been determined to be the combination of an MAA/SPI mass ratio of 3:4, 0.8 g of SHMP, and 0.2 g of KPS, reacted for 30 min at 60 ℃. The dust suppressant prepared under the determined optimal process conditions exhibits good adhesion and compression performance. It can effectively prevent dust from becoming airborne and creating air pollution.

3.2 SEM and EDS Analysis

To clearly observe the microscopic state of the interaction between the dust suppressant and the sprayed coal dust, SEM observations and EDS elemental analysis were conducted, as shown in Fig. 4–6. Figure 4a shows an SEM image of the morphology of the dust suppressant at 300· magnification. It can be seen that the droplets of the dust suppressant look like spherical particles with depressions on the

surface, similar in shape but with different sizes. Figure 4b shows the morphology of the solidified shell formed by the dust suppressant on the surface of the coal sample at 300· magnification. It can be seen that the dust suppressant droplets are fused together, and the dust suppressant droplets combine with the coal dust to effectively wrap the coal dust particles in the coal. A dense cured film is formed on the dust surface. Figure 4c shows the morphology of the combination of dust suppressant and coal dust at 10,000· magnification. It can be seen that the coal dust and dust suppressant are bonded and cross-linked together, and the dust suppressant droplets can effectively bond to coal dust particles, showing strong adhesion. Figure 4d shows that the dust suppressant forms a dense dust suppression film on the surface of coal dust, and the coal dust particles are covered underneath. The clear outline of the coal dust particles can be seen from the circled position. This dust suppression film has notable compressive strength and is able to resist wind erosion and prevent the coal dust from becoming airborne.

Figure 6 EDS and elemental surface distribution map of solidified layer of dust suppressant

3.3 FTIR Spectra Analysis

Figure 7 shows the FTIR spectra of SPI, the SPI-MAA intermediate product, and the dust suppressant synthesized by SPI-MAA-SHMP. In the FTIR spectrum of SPI, the peaks at 3435 and 1654 cm^{-1} correspond to the O-H and N-H stretching vibration peaks of the hydroxyl and amide groups, respectively. The characteristic peaks of the amide I band at 1032 cm^{-1} belong to the C = O stretching vibration of the carbonyl group in the SPI. The FTIR spectra of the modified forms of SPI, SPI-MAA, and SPI-MAA-SHMP can be compared with the SPI spectrum. Regardless of the peak position or shape, the FTIR spectra of all three materials are similar. Therefore, it can be preliminarily judged that the synthesis of the dust suppressant is successful. The peak position at 3400 cm^{-1} is roughly the same for all three materials, but the peak position gradually shifts to the right. The shift is due to the graft copolymerization between the SPI and MAA monomers. The intensity of the absorption peak near 1650 cm^{-1} in the SPI-MAA and SPI-MAA-SHMP spectra gradually decreases. The decrease suggests that after SPI participates in the reaction, its active groups are consumed. The characteristic absorption peak of the cross-linker SHMP at 987 cm^{-1} shows that SHMP successfully participated in the reaction to form a dust suppressant with a network structure [28–30].

3.4 DSC Analysis

SPI is a protein with a naturally formed structure. Chemical polymerization causes the protein to undergo a transformation. DSC is used to measure the thermal denaturation temperature of the protein and to evaluate whether the graft copolymerization modification of SPI is successful.

Figure 8 shows the DSC curves of SPI, SPI-MAA, and SPI-MAA-SHMP in the liquid and solid states. To clearly see the peak changes, a section of Fig. 8a is enlarged to make Fig. 8b. It can be seen in Fig. 8b that with the continuous modification of SPI, the melting peak shifts toward higher temperatures, and the melting peak temperature of the same substance in the liquid state is slightly greater than the solid melting peak, i.e. $T_{SPI-L} > T_{SPI-S}$, $T_{SPI-MAA-L} > T_{SPI-MAA-S}$, and $T_{SPI-MAA-SHMP-L} > T_{SPI}$. The shift in melting

temperature occurs because the liquid substance contains water, which causes the melting peak to shift to the right during the heating and evaporation process. The melting peak of SPI-S is 101.85 ºC. After adding MAA, the melting peak of SPI-MAA-S is 111.36 ℃, and the melting peak shifts to the right. The shift may be due to the graft copolymerization of SPI and MAA. More energy is required to melt the connected SPI-MAA than the SPI, which is manifested as a shift of the melting peak to higher temperatures. Similarly, after cross-linking with SHMP, the melting peak of the product SPI-MAA-SHMP continues to shift to higher temperatures, and the melting peak of SPI-MAA-SHMP-S is 115.57°C. The change in melting temperature is caused by the increase in molecular weight after cross-linking, which can lead to the increase of denaturation temperature of cross-linked proteins [31, 32].

3.5 Analysis of TSP Results

Table 1
Weather report during the monitoring periods

Date	Temperature /°C	Wind /degree	Direction of wind
2020/11/2	4–18	5–6	North
2020/11/3	2–12	4–5	North
202011/4	7–14	3–4	South
2020/11/5	11–16	3–4	West-south

Figure 9 shows the TSP monitoring data of the test group and the control group at the monitoring points over 4 days, and Table 1 shows the weather conditions during the monitoring period. On the second and third days, the wind was strong, and the TSP value of monitoring point 1 in the control group was higher. The maximum TSP value of 9.1 μg/m^3 occurred at 18:00 on the second day. According to the data analysis, the average TSP of monitoring point 1 in the control group over 4 days was 5.18 μg/m^3. The average TSPs at monitoring point 2 and the downwind monitoring point 3 in the experimental group over 4 days were 1.80μg/m^3 and 1.85μg/m^3, respectively. Compared with the control group, the experimental group had an average TSP reduction of 79.95%. This finding showed that spraying of the dust suppressant can effectively fix the coal dust on the surface of the coal pile. The consolidation layer formed by spraying the dust suppressant can effectively prevent the coal powder from being blown aloft by the wind and can therefore reduce air pollution.

4. Dust Suppression Mechanism

SPI has a relatively complex and stable polymer structure. The forces supporting the protein structure include hydrogen bonds, disulfide bonds, and electrostatic bonds [33–35]. However, this stable structure can be handled by chemical modification methods. Appropriate modification can strengthen the intermolecular and intramolecular forces and enhance the mechanical properties of the SPI membrane. Modification can also enhance the stability of the network structure in the protein membrane and improve the performance of the membrane. The dust suppressant synthesis process first disperses the SPI solid

powder in a urea solution. Urea can promote the SPI chain structure to become relatively expanded, so that the SPI polymer chain exposes more functional groups, such as -COOH and -NH_2. The stretching of the SPI chain structure facilitates the grafting reaction, as shown in Fig. 10.

Under the action of the initiator KPS, the monomer MAA and the exposed main groups of SPI undergo a graft copolymerization reaction, as shown in Fig. 11. The added cross-linking agent SHMP promotes the formation of a network structure between high molecular weight polymers. This cross-linked network structure has a strong cohesive force. It can effectively capture coal dust and accomplish coal dust suppression. The mechanism of the reaction process is shown in Fig. 12 [36, 37].

5. Conclusion

To suppress the dust pollution in an open-air environment, improve the surrounding atmospheric environment, and improve the environmental quality, this research created a dust suppressant that effectively suppresses dust from becoming airborne. A graft copolymerization reaction between SPI and MAA was developed using the initiator KPS and the cross-linking agent SHMP to create a dust suppressant with a cross-linked network structure. The main conclusions are as follows:

(1) The method of controlling single variables was used to test the viscosity and compressive strength of each factor to determine the best process conditions for the synthetic dust suppressant, which were: MAA/SPI mass ratio = 3:4, SHMP cross-linking agent: 0.8 g, KPS Initiator: 0.2 g, 60 ℃ grafting reaction 30 min.

(2) As confirmed with SEM, EDS, FTIR, and DSC characterization of the dust suppressant and on-site TSP monitoring, the graft copolymerization of SPI and MAA was successfully achieved. The synthesized dust suppressant was bonded and cross-linked on the surface of the coal pile, and the bonding force was relatively good. The dust suppressant formed a strong and dense solidified layer, which effectively prevented dust from being blown off a coal pile. Compared with an untreated coal pile, the average reduction of the TSP in the coal pile sprayed with dust suppressant was 79.95%, showing a significant dust suppression effect.

(3) The main raw material SPI used in the experiment is a natural renewable polymer material with a wide range of sources and is biodegradable. The developed dust suppressant is in line with the theme of environmental friendliness and green processes and materials.

Declarations

Acknowledgements

This work has been funded by the National key R & D plan for the 13th five year plan(2017YFC0805200), the Qingdao science and technology plan project (19-3-2-6-zhc), the Natural Science Foundation of Shandong Province (ZR2019MEE118), the National Natural Science Foundation of China (51974179).

Conflict of Interest

The authors declare no conflict of interest.

References

1. Alejandro B, Mariajosé C, Juan PC, Guillermo EC, Mariano E (2020) Rheological Characterization of a Wood Adhesive Based on a Hydrolyzed Soy Protein Suspension. J Polym Environ 28:2490–2497. https://doi.org/10.1007/s10924-020-01784-x
2. Bao Q, Nie W, Liu CQ, Liu YH, Zhang HH, Wang HK, Jin H (2019) Preparation and characterization of a binary-graft-based, water-absorbing dust suppressant for coal transportation. J Appl Polym Sci 136:47065. http://dx.doi.org/10.1002/app.47065
3. Mita C, Bunea I, Roman T, Humelnicu D (2021) Cross-Linked and Functionalized Acrylic Polymers: Efficient and Reusable Sorbents for Zn(II) Ions in Solution. J Polym Environ. https://doi.org/10.1007/s10924-020-02005-1
4. Fan T, Liu ZY, Ouyang JT, Li MZ (2020) Synthesis and performance characterization of an efficient coal dust suppressant for synergistic combustion with coal dust. J ENVIRON MANAGE 269:110854. https://doi.org/10.1016/j.jenvman.2020.110854
5. Hua Y, Nie W, Wei WL, Liu Q, Liu YH, Peng HT (2018) Research on multi-radial swirling flow for optimal control of dust dispersion and pollution at a fully mechanized tunnelling face. Tunn Undergr Sp Tech 79:293–303. http://dx.doi.org/10.1016/j.tust.2018.05.018
6. Jin H, Nie W, Zhang HH, Liu YH, Bao Q, Wang HK, Huang DM (2018) The preparation and characterization of a novel environmentally-friendly coal dust suppressant. J ApplPolymer Sci 136:47354. http://dx.doi.org/10.1002/app.47354
7. Jin H, Nie W, Zhang YS, Wang HK, Zhang HH, Bao Q, Yan JY (2019) Development of environmental friendly dust suppressant based on the modification of soybean protein isolate. Processes 7:165. http://dx.doi.org/10.3390/pr7030165
8. Luo RD, Lin MS, Luo YB, Dong JF (2016) Preparation and properties of a new type of coal dust suppressant. Journal of China Coal Society 41:454–459. https://doi.org/10.13225/j.cnki.jccs.2015.1303
9. Nie W, Wei WL, Ma X, Liu YH, Peng HT, Liu Q (2017) The effects of ventilation parameters on the migration behaviors of head-on dusts in the heading face.Tunn. Undergr Sp Tech 70:400–408. http://dx.doi.org/10.1016/j.tust.2017.09.017
10. Nie W, Liu YH, Wang H, Wei WL, Peng HT, Cai P, Hua Y, Jin H (2017) The development and testing of a novel external-spraying injection dedusting device for the heading machine in a fully-mechanized excavation face. Process Saf Environ Prot 109:716–731. http://dx.doi.org/10.1016/j.psep.2017.06.002
11. Zhang HH, Nie W, Liu YH, Wang HK, Jin H, Bao Q (2018) Synthesis and performance measurement of environment-friendly solidified dust suppressant for open pit coalmine. J Appl Polym Sci 135:46505.

http://dx.doi.org/10.1002/app.46505

12. Zhang HH, Nie W, Wang HK, Bao Q, Jin H, Liu YH (2018) Preparation and experimental dust suppression performance characterization of a novel guar gum-modification-based environmentally-friendly degradable dust suppressant. Powder Technol 339:314–325. http://dx.doi.org/10.1016/j.powtec.2018.08.011
13. Luo LH, Liang H, Gong WR, Yang L, Yu YM, Tian WQ, Chen Y (2012) Effects of Storage Conditions on the Structure and Properties of Cellulose/Soy Protein Isolate Composite Membranes. Journal of Wuhan University(Natural Science Edition) 58:302–306. http://dx.doi.org/10.14188/j.1671-8836.2012.04.005
14. Ma MX, Liu R, Liu HQ, Gu YJ (2020) Study on $LiFe_{0.2}Mn_{0.8}PO_4$/C cathode materials coated with different carbon contents. Journal of Shandong University of Science Technology(Natural Science) 39:1–7. https://doi.org/10.16452/j.cnki.sdkjzk.2020.06.005
15. Saha P, Ksaibati K (2020) Effectiveness of the two chemical treatments ($CaCl_2$ and $MgCl_2$) as dust suppressants on gravel roads. Int J Pavement Eng. http://dx.doi.org/10.1080/10298436.2020.1745799
16. Hu Y, Shi L, Shan ZH, Dai R, Chen H (2020) Efficient removal of atmospheric dust by a suppressant made of potato starch, polyacrylic acid and gelatin. Environ Chen Lett 18:1701–1711. http://dx.doi.org/10.1007/s10311-020-01025-6
17. Xie ZH, Li XC (2012) Research on complex dust suppressants for transport roadways in open mines. Chinese Journal of Engineering 11:1240–1244. http://dx.doi.org/10.13374/j.issn1001-053x.2012.11.004
18. Li YQ, Dong B, Cai JX, Zhao BW, Li X (2019) Research on performance characterization and application of the composite dust suppressant for pulverized coal. Journal of Lanzhou Jiaotong University Chinese Journal of Engineering 38:105–113. http://dx.doi.org/10.3969/j.issn.1001-4373.2019.05.016
19. Wang XJ, Wang RM, He YF, He NP (2011) Advanced on Modification and Application of Soy Protein Isolate. Chemistry 5:396–401. http://dx.doi.org/10.14159/j.cnki.0441-3776.2011.05.003
20. Lu XS, Li R, Li N, Sun WJ (2017) Study on the Preparation of Hydrogel and Its Properties by the Grafting of Methacrylic Acid Graft Modified Soy Protein Isolate. Journal of Gansu Normal Colleges 22:34–37
21. China Industry Information Network 2020: 2020–2026 China's soybean industry market operation potential and marketing channel analysis report http://www.chyxx.com/industry/202004/857598.html
22. Luo DH (2020) Functional properties of modified soybean protein by homogenous. South China University of Technology
23. Huang JN, Liu JX, Xue D (1997) Functional characteristics and modification trend of soybean protein. The Food Industry 3:8–11

24. Wang D, Dai L, Gao YX (2018) Progress in Enzymatic Modification of Proteins. Food Science 39:233–239. http://dx.doi.org/10.7506/spkx1002-6630-201815034
25. Si YH (2012), Effect of uitrafine communitation on function of soybean protein isolate. Shandong Agricultural University
26. Tian K, Guan J, Shao ZZ, Chen X (2018) Structural and Functional Study of Soybean Protein Isolation. Progress in Chemistry 4:565–573
27. Yang SN (2015) Then influence of different processing technology of functional properties of SPI and its components.Heilongjiang Bayi Agricultural University
28. Podaralla S, Averineni R, Alqahtani M, Perumal O (2012) Synthesis of novel biodegradable methoxy poly (ethylene glycol) -zein micelles for effective delivery of curcumin. Mol Pharmaceut 9:2778–2786. http://dx.doi.org/10.1021/mp2006455
29. Dockal M, Carter DC, Ruker F (2000) Conformational transitions of the three recombinant domains of serum albumin depending on pH. J Biol Chem 275:3042–3050. http://doi.org/10.1074/jbc.275.5.3042
30. Andreia V, Freddi G, Cavaco-Paulo A (2008) Biodegradable materials based on silk fibroin and keratin. Biomacromolecules 9:1299–1305. https://doi.org/10.1021/bm7012789
31. Carafa M, Marianecci C, Luisa DM, Federica R, Chiara DM, Pietro M, Franco A, Tommasina C (2011) A new vesicle-loaded hydrogel system suitable for topical applications: preparation and characterization. J Pharm Pharm Sci 14:336–346. https://doi.org/10.18433/J3160B
32. Nishinari K, Fang Y, Guo S, Phillipsa GO (2014) Soy proteins: A review on composition, aggregation and emulsification. Food Hydrocolloids 39:301–318. http://dx.doi.org/10.1016/j.foodhyd.2014.01.013
33. Hsieh JF, Yu CJ, Chang JY, Chen ST, Tsai HY (2014) Microbial transglutaminase-induced polymerization ofβ-conglycinin and glycinin in soymilk: a proteomics approach. Food Hydrocolloids. 35: 678–685. https://doi.org/10.1002/1097-4636(20001215)52:4<577::AID-JBM1>3.3.CO;2-X
34. Mitra BC (2014) Environment friendly composite materials: biocomposites and green composites. Defence Sci J 64:244–261. https://doi.org/10.14429/dsj.64.7323
35. Garrido T, Etxabide A, Peñalba M, Caba K, Guerrero P (2013) Preparation and characterization of soy protein thin films: Processing–properties correlation. Mater Lett 105:110–112. https://doi.org/10.1016/j.matlet.2013.04.083
36. A.S. Hoffman, P.S. Stayton, V. Bulmus, et al., (2000) Really smart bioconjugates of smart polymers and receptor proteins. J Biomed Mater Res A, 52: 577–586. https://doi.org/10.1002/1097-4636(20001215)52:4<577::AID-JBM1>3.0.CO;2-5
37. Owens DE, Jian YC, Fang JE, Slaughter BV, Chen YH, Peppas NA (2007) Thermally responsive swelling properties of polyacryla-mide/poly (acrylic acid) interpenetrating polymer network nanoparticles. Macromolecules 40:7306–7310. https://doi.org/10.1021/ma071089x

Figures

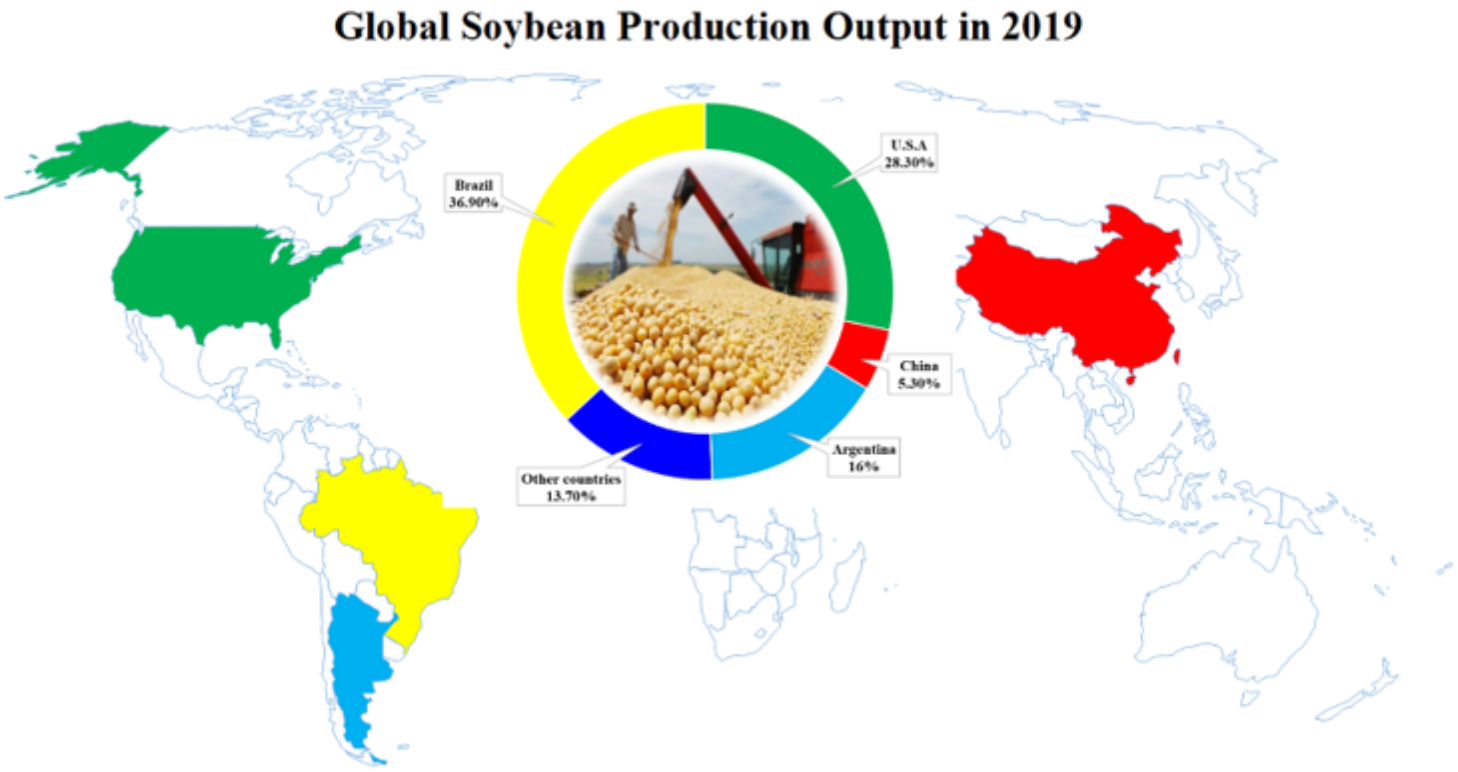

Figure 1

The output of major soybean producing countries in 2019. Note: The designations employed and the presentation of the material on this map do not imply the expression of any opinion whatsoever on the part of Research Square concerning the legal status of any country, territory, city or area or of its authorities, or concerning the delimitation of its frontiers or boundaries. This map has been provided by the authors.

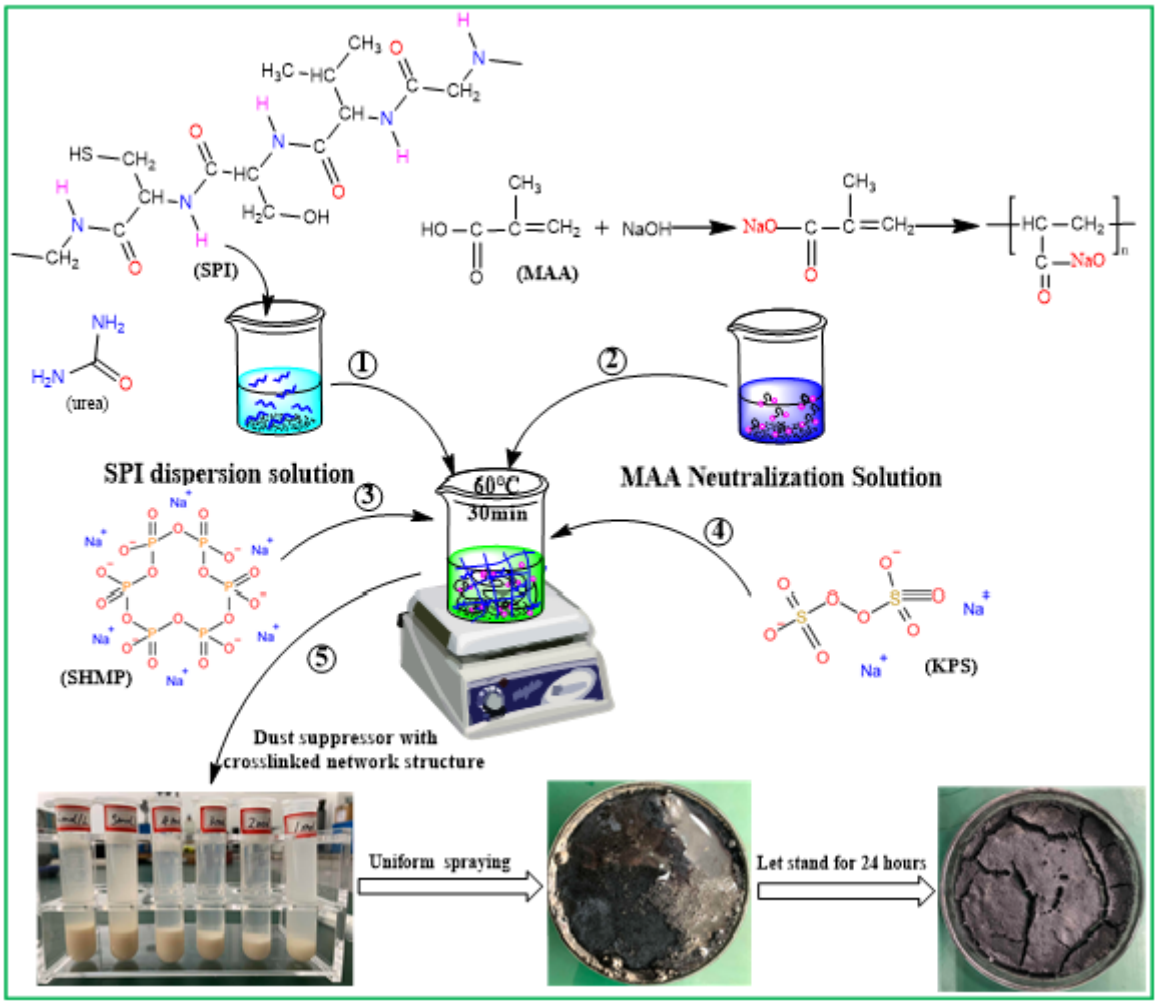

Figure 2

Flow chart of synthesis of dust suppressant with a cross-linked structure

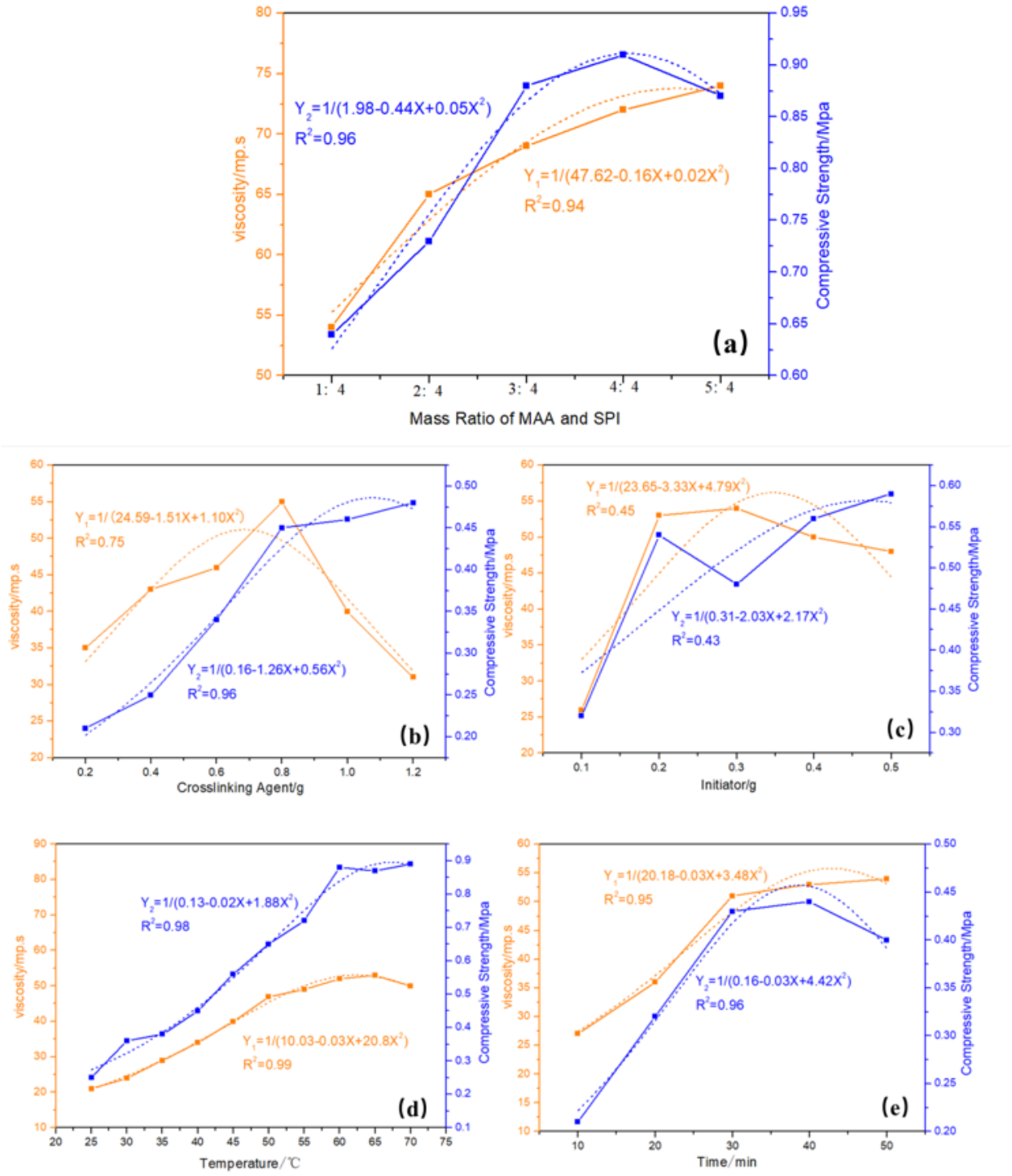

Figure 3

Influence data of single factor on the performance of dust suppressant

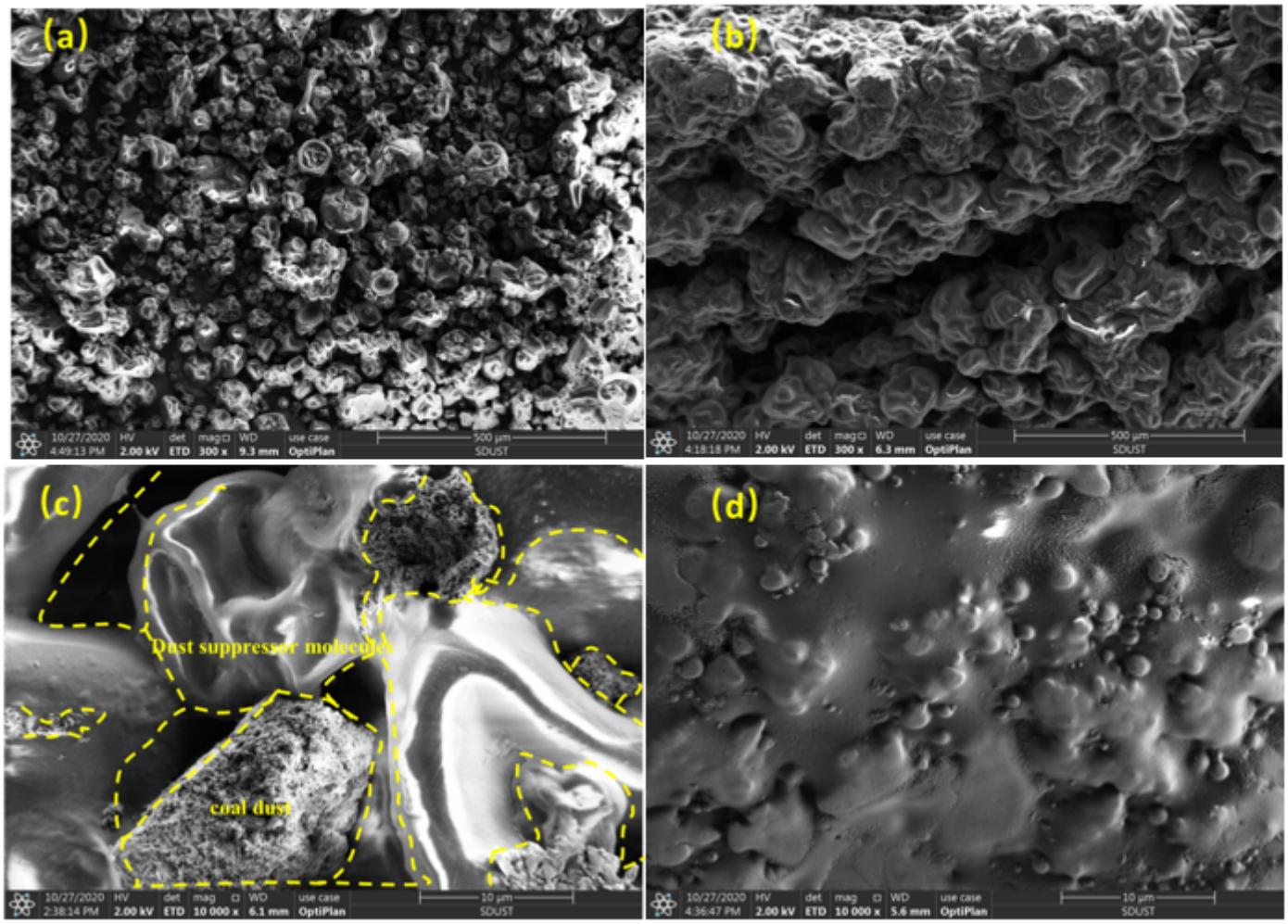

Figure 4

(a) SEM image of dust suppressant (b), (c), (d) SEM images of cured dust suppressant shell at different magnifications

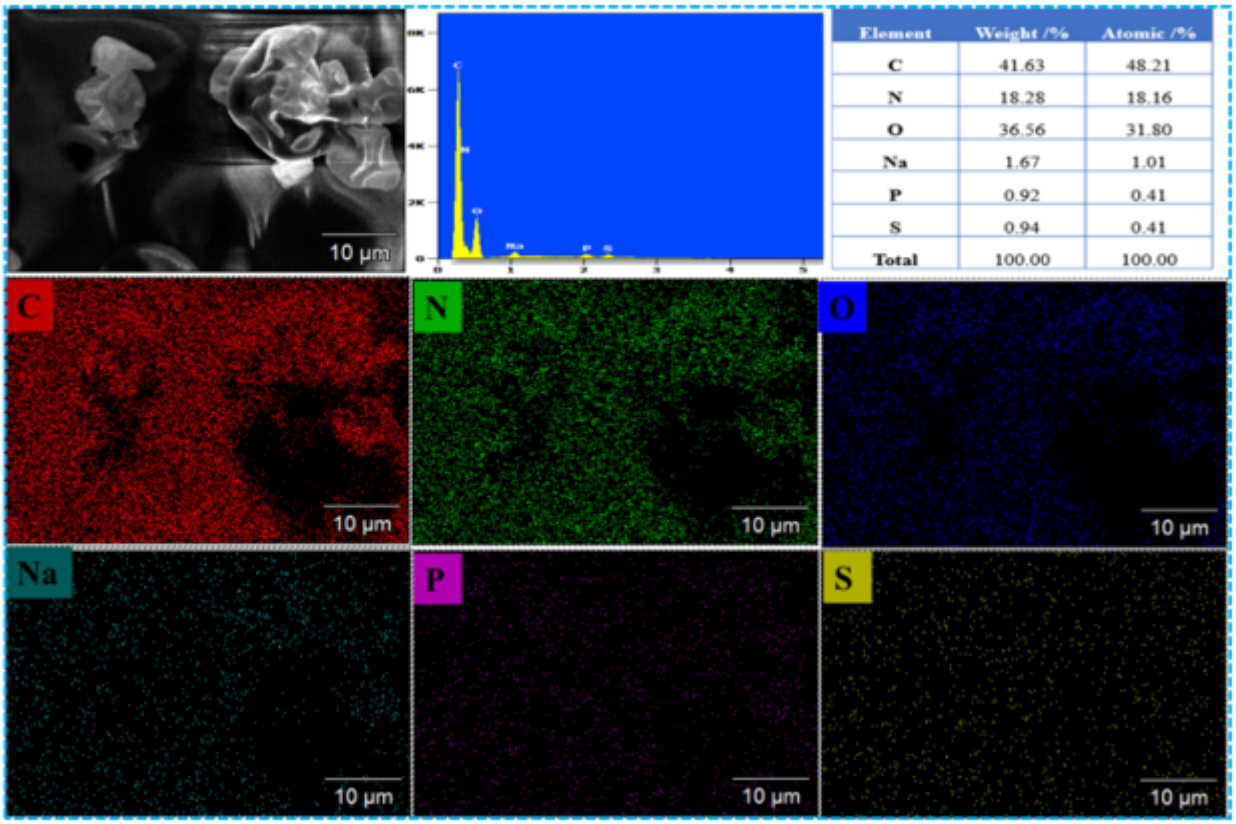

Element	Weight /%	Atomic /%
C	41.63	48.21
N	18.28	18.16
O	36.56	31.80
Na	1.67	1.01
P	0.92	0.41
S	0.94	0.41
Total	100.00	100.00

Figure 5

EDS and elemental surface distribution map of soy protein isolate

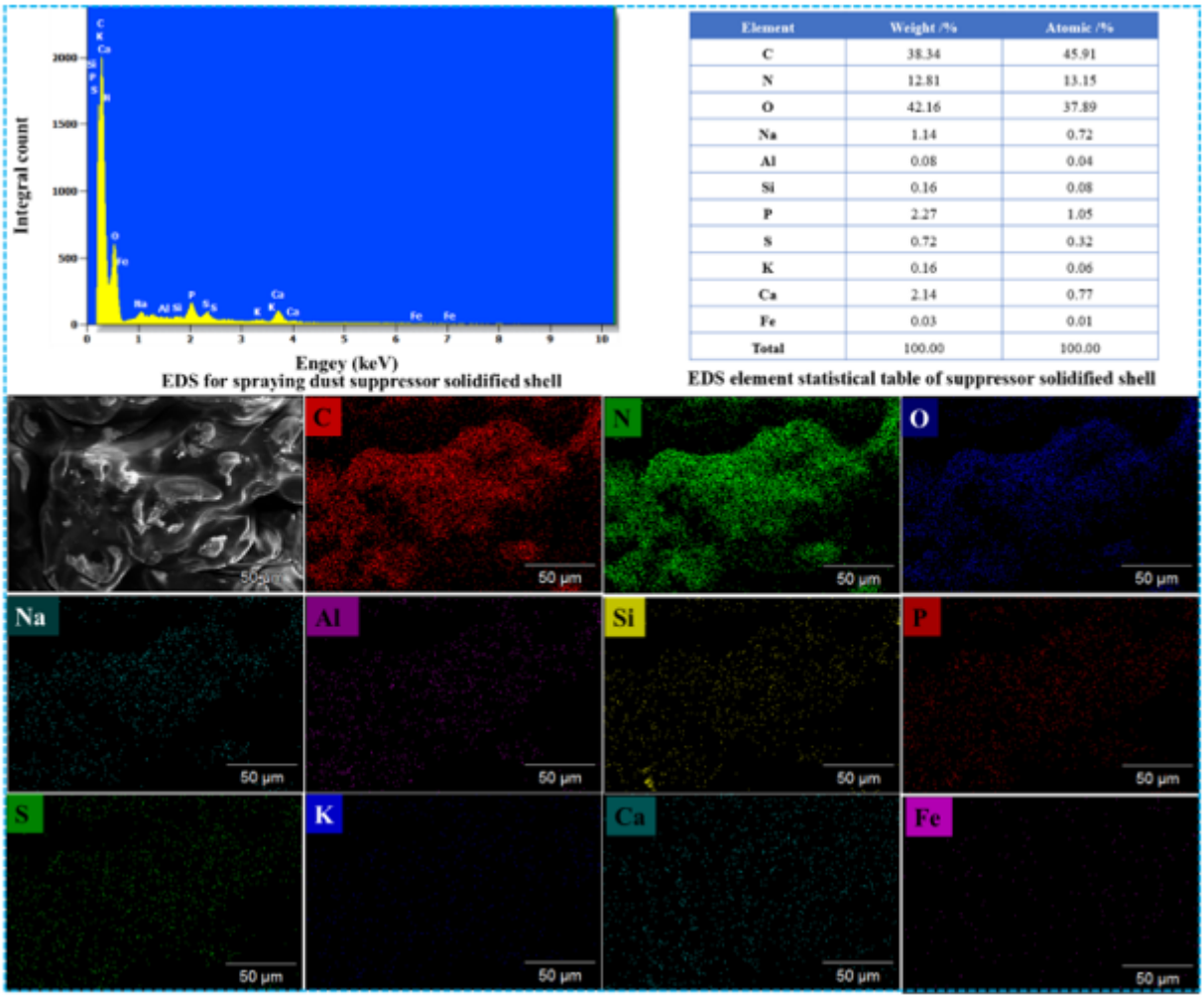

Element	Weight /%	Atomic /%
C	38.34	45.91
N	12.81	13.15
O	42.16	37.89
Na	1.14	0.72
Al	0.08	0.04
Si	0.16	0.08
P	2.27	1.05
S	0.72	0.32
K	0.16	0.06
Ca	2.14	0.77
Fe	0.03	0.01
Total	100.00	100.00

Figure 6

EDS and elemental surface distribution map of solidified layer of dust suppressant

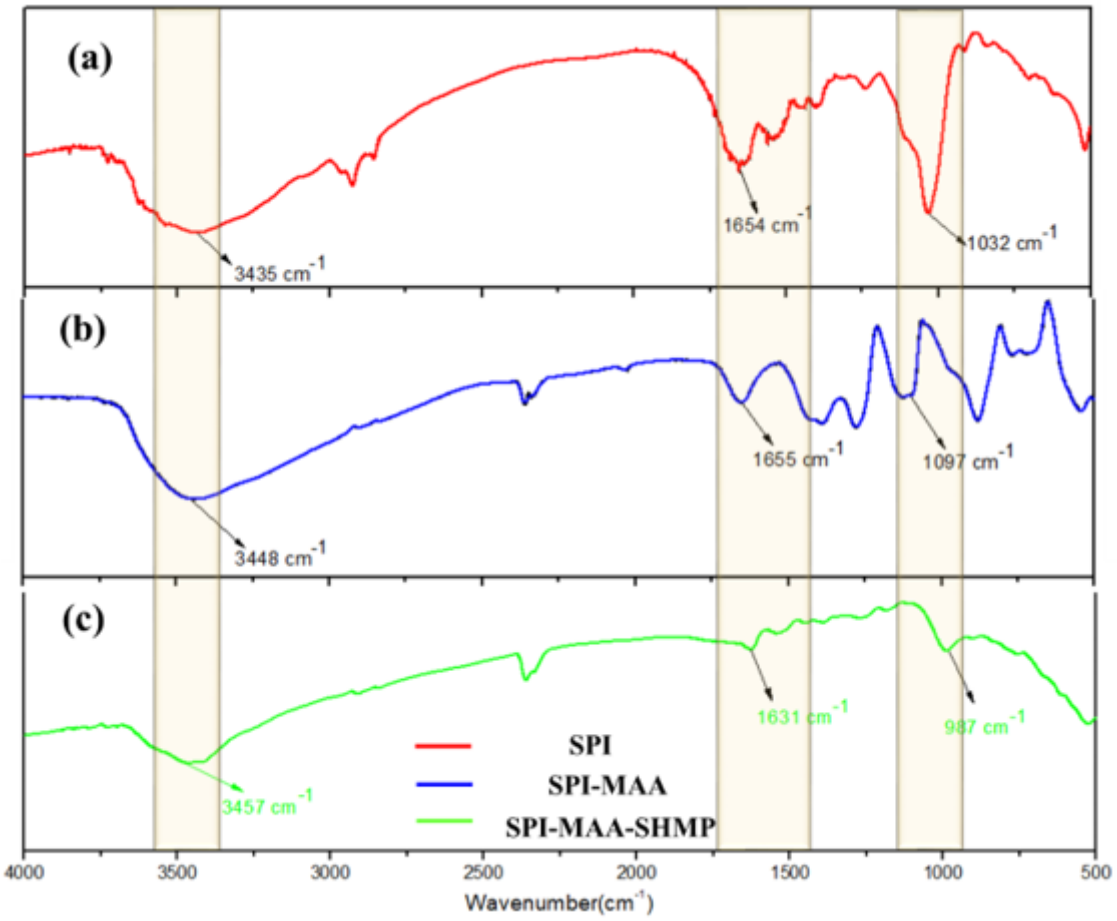

Figure 7

FTIR spectra of SPI, SPI-MAA, and SPI-MAA-SHMP

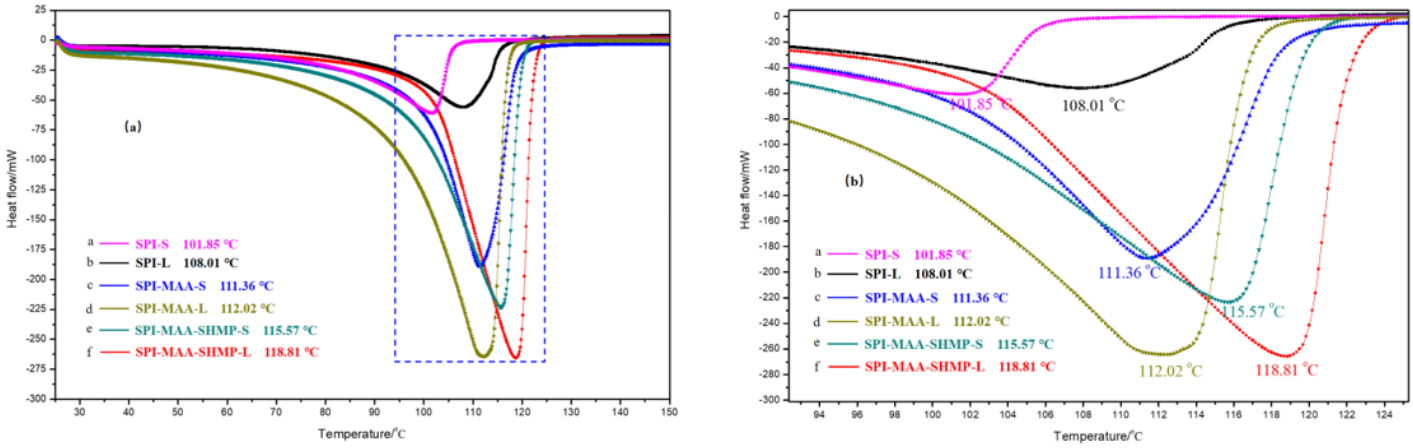

Figure 8

(a) DSC curves of SPI, SPI-MAA and SPI-MAA-SHMP in the solid (-S) and liquid (-L) state (b) An enlarged view of the curve outlined by the blue dashed box in (a)

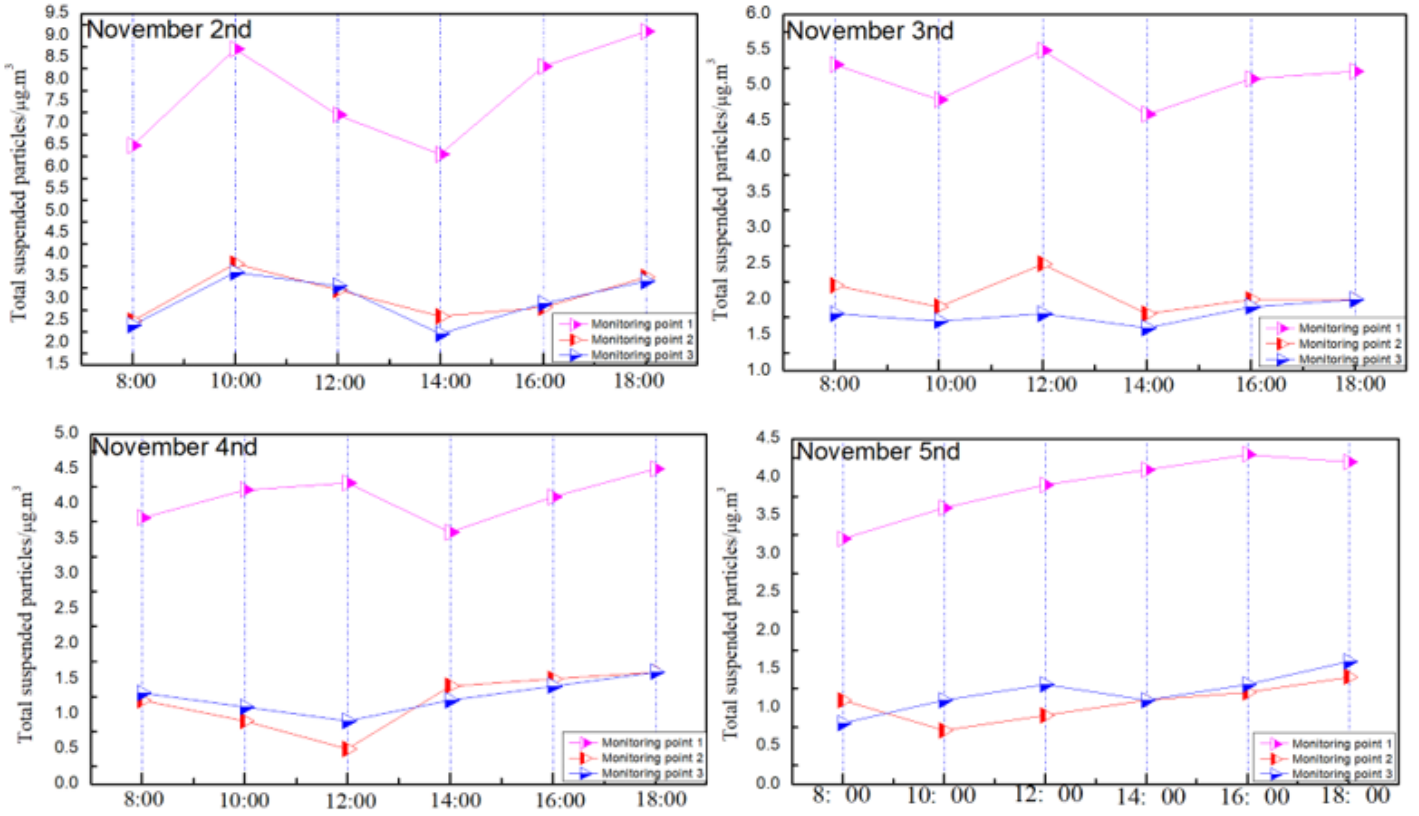

Figure 9

Total suspended particulate (TSP) value of coal pile monitoring in an open-air environment

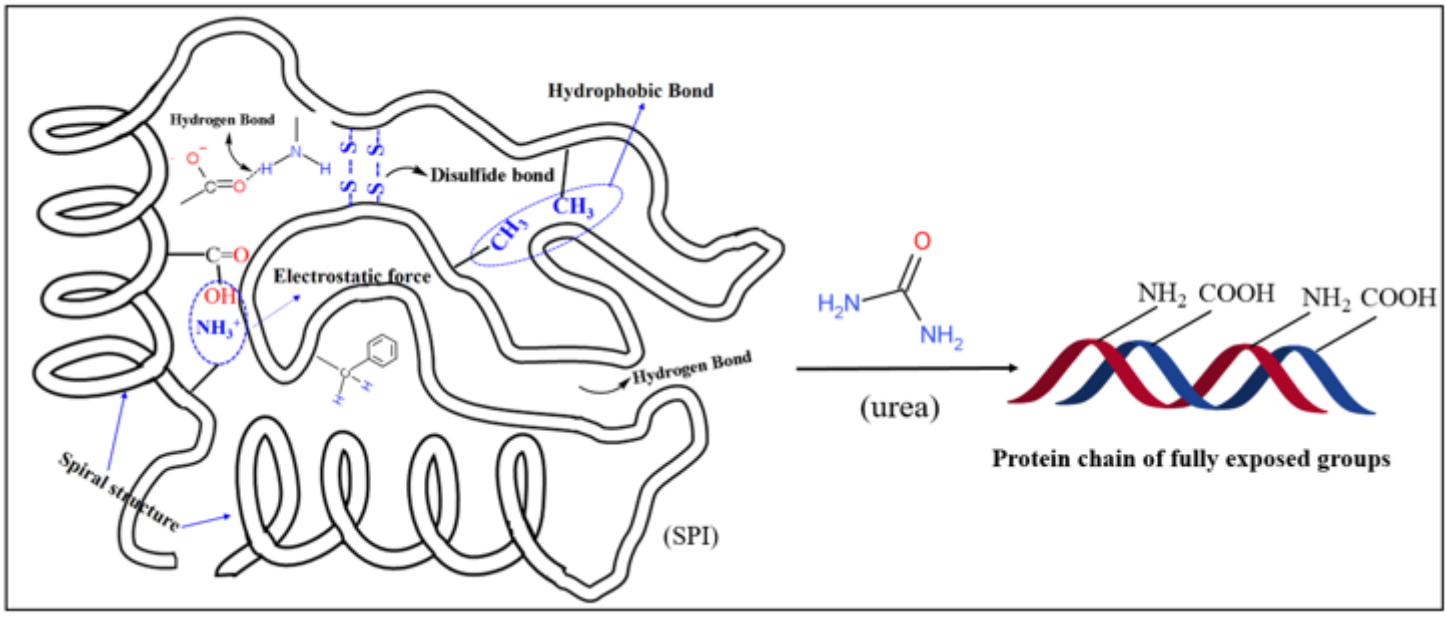

Figure 10

Urea promotes stretching of the soy protein isolate (SPI) chain

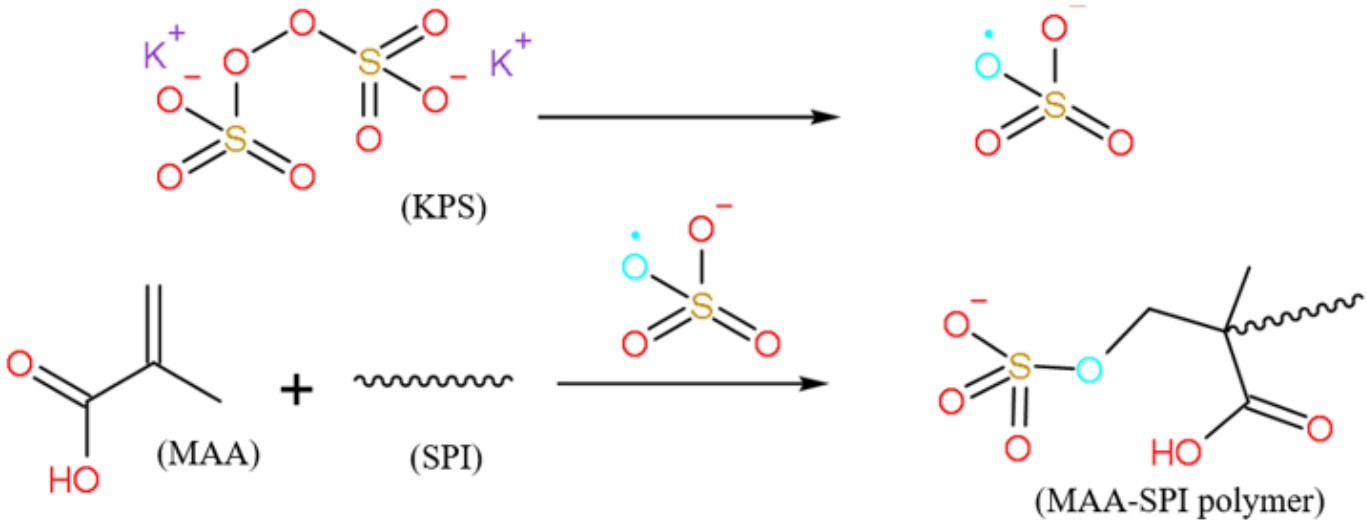

Figure 11

KPS initiates graft copolymerization of SPI and MAA

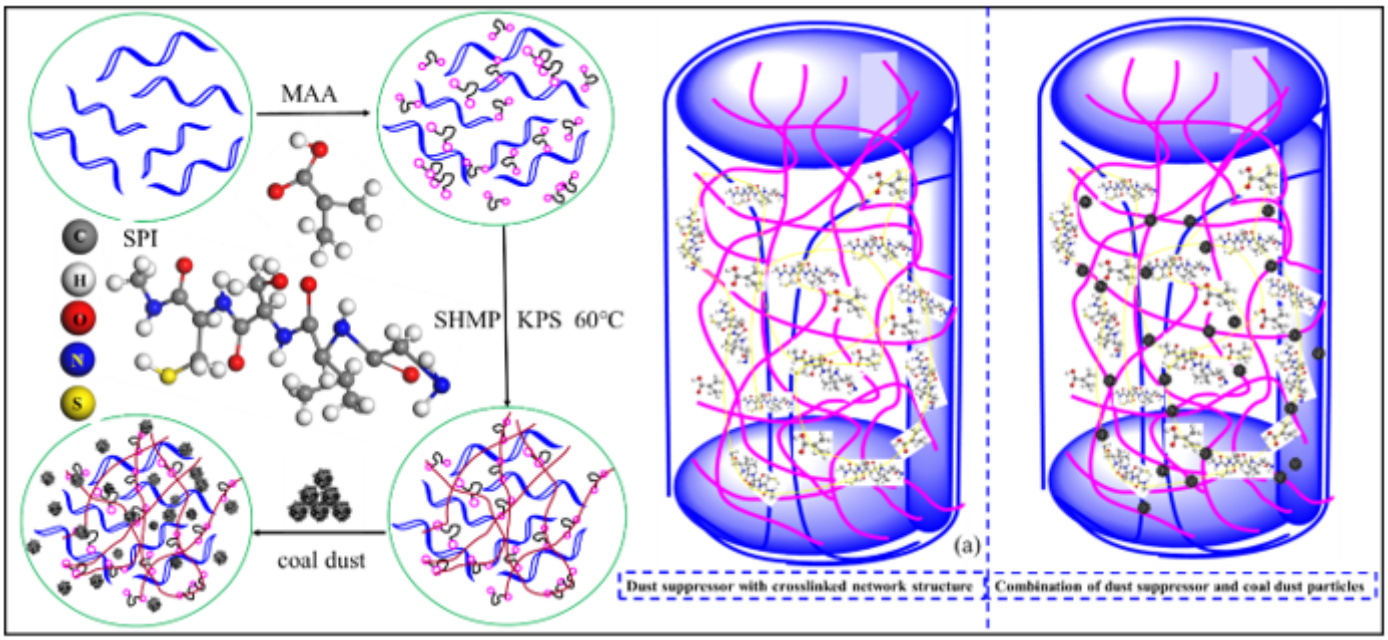

Figure 12

Diagram of the synthesis and mechanism of the dust suppressant with a cross-linked structure

Supplementary Files

This is a list of supplementary files associated with this preprint. Click to download.

- Highlights.docx
- GraphicalAbstracts.docx